Resonant tunnelling in nc-Si/SiO_2 multilayers at room temperature*

Chen Deyuan(陈德媛)[1,2,†]

[1]College of Electronic Science & Engineering, Nanjing University of Posts and Telecommunications, Nanjing 210046, China
[2]Nanjing National Laboratory of Microstructures and Key Laboratory of Advanced Photonic and Electronic materials, Department of Physics, Nanjing University, Nanjing 210093, China

Abstract: Nc-Si/SiO_2 multilayers were fabricated on silicon wafers in a plasma enhanced chemical vapour deposition system using *in situ* oxidation technology, followed by three-step thermal treatments. Carrier transportation at room temperature is characterized by current voltage measurement, and negative different conductances can be observed both under forward and negative biases, which is explained by resonant tunnelling. The resonant tunnelling peak voltage is related to the thicknesses of the nc-Si and SiO_2 sublayers. And the resonant tunnelling peak voltage under negative bias is larger than that under forward bias. An energy band diagram and an equivalent circuit diagram were constructed to analyze and explain the above transportation process and properties.

Key words: resonant tunnelling; work function; quantum dots
DOI: 10.1088/1674-4926/32/8/083004 **PACC:** 7335C; 7340C; 7320D

1. Introduction

Silicon quantum dots have been studied for years and many properties overmatching bulk silicon have been discovered. Except high efficient light emission properties[1−4], carrier transport in nc-Si such as Fowler–Nordheim (F–N) tunneling[5,6], direct tunneling and resonant tunneling. Special carrier transport, such as resonant tunnelling due to energy level quantization in the quantum well, drives scientists to construct new devices called resonant tunnelling devices (RTDs)[7−9], etc. It is known that resonant tunneling originates from energy level quantization in a quantum well confined between materials of larger band gap. When tunnelling takes place, injection carriers with energy equal to the quantized energy level in the quantum well tunnel and the energy barrier and drive current flow across the devices. The RTDs possess many properties, such as low power consumption, high speed and multiple stable states, making them promising for nanoelectronic applications[10,11]. It should be pointed out that the confinement materials play important roles in the properties of the devices, and many materials could be chosen for this role, such as SiC_x, SiN_x and SiO_x, or others with a large band gap. Resonant tunnelling in the nc-Si/SiN_x system has been reported previously[7]. The peak to valley current ratio (PVCR) differs greatly under illumination and dark, reaching to 2240 and 390, respectively. In comparison with SiN_x, SiO_2 dominates as a barrier material. First, SiO_2 can adhere to Si well and provide better interface characteristics; second, the fabrication process is compatible with the microelectronic process; third, the band gap is about 8.9 eV, greater than that of SiN_x, making multiple resonant tunnelling possible. So we choose SiO_2 as the confinement material. Nc-Si/SiO_2 multilayers were fabricated to form multi-barriers and resonant tunnelling was studied in a dark room.

2. Experiments

The samples were deposited in a plasma enhanced chemical vapour deposition system[12], alternating amorphous silicon (α-Si) deposition and *in situ* oxidation processes, as shown in Fig. 1. The radio frequency is 13.56 MHz and the deposition temperature is kept at 250 ℃. The as-deposited samples were annealed step-by-step (dehydrogenation at 400 ℃ for 40 min; rapid thermal annealing at 1100 ℃ for 50 s; furnace annealing at 1000 ℃ for 40 min). The α-Si crystallized during annealing. Then aluminum was vaporized on both surfaces of the samples as the electrode contact, as shown in Fig. 1. In the current work, p-type crystal silicon wafers were used as substrates. The α-Si deposition time was set to 10 s, and the *in situ* oxidation time was set to 20 s (for sample A) and 10 s (for sample B), respectively, in comparison. Eight periods of nc-Si/SiO_2 were fabricated. The current voltage curves were measured at room temperature using an Agilent 4156C semiconductor parameter

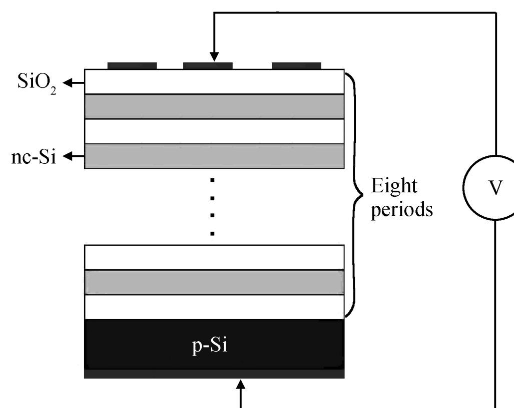

Fig. 1. Structure sketch of the nc-Si/SiO_2 multilayers.

* Project supported by the Jiangsu Provincial Foundation for Youths, China (No. 09KJB510008) and the Research Foundation for Advanced Talents of Nanjing University of Post and Telecommunications, China (No. NY208056).
† Corresponding author. Email: chendy@njupt.edu.cn
Received 28 January 2011, revised manuscript received 26 March 2011
© 2011 Chinese Institute of Electronics

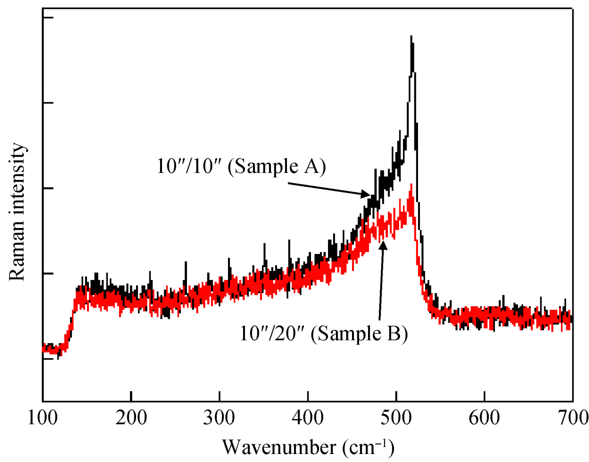

Fig. 2. Raman scattering curves for samples A and B.

analyzer and an Agilent 4284A LCR meter.

3. Results and discussion

The microstructures of samples A and B were characterized by measurement of Raman scattering spectra in Fig. 2. The transverse optical (TO) vibration mode in the nc-Si grain was about 517.5 and 518.6 cm^{-1}, respectively. The TO mode for single crystal silicon was 521 cm^{-1}. According to the phonon confinement model[13],

$$d = 2\pi\sqrt{\frac{B}{\Delta\omega}}, \quad (1)$$

where d is the grain diameter, $B = 2.24$ nm^2/cm is a constant, and $\Delta\omega$ is the frequency shift of the TO mode in the nc-Si grain than that in the single crystal silicon. From Eq. (1), the diameters of the nc-Si grains are 5.0 and 6.0 nm, respectively, for samples A and B.

Figure 3(a) shows the current voltage characteristics for samples A and B. Resonant tunnelling peaks can be observed under both forward and negative biases. For sample A, the resonant tunnelling peak voltage (RTPV) is about 3 V and the peak to valley current ratio (PVCR) is nearly 2 under forward bias; the corresponding values are 9 V and 1.1 under negative bias from resonant tunnelling data in Fig. 3(b). For sample B, the RTPV values are 1.8 V and 7.5 V, and the PVCR values are 4 and 1.25, respectively, under forward and negative biases. The PVCR values are greater for sample B than for A, and this may be related to the width of quantized energy sub band in the quantum well confined by the finite SiO_2 barrier. Outside of the resonant tunnelling peak, the current is not zero and increases with applied bias, caused by the other types of transportation mechanisms, such as FN tunneling and direct tunneling. These mechanisms dominate the transportation process in different electric field regions[14].

In this paper, we discuss the electron transportation process only. The resonant voltage V_p is expressed as[15]

$$E_n = \frac{\hbar^2 k_x^2}{2m^*} = \frac{h^2 n^2}{8m^* W_{well}^2}, \quad (2)$$

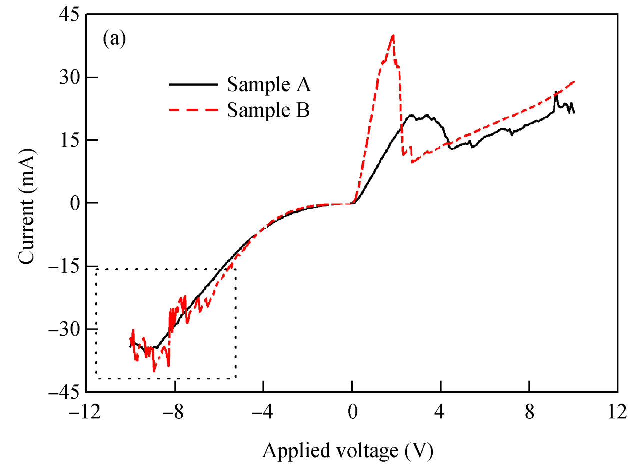

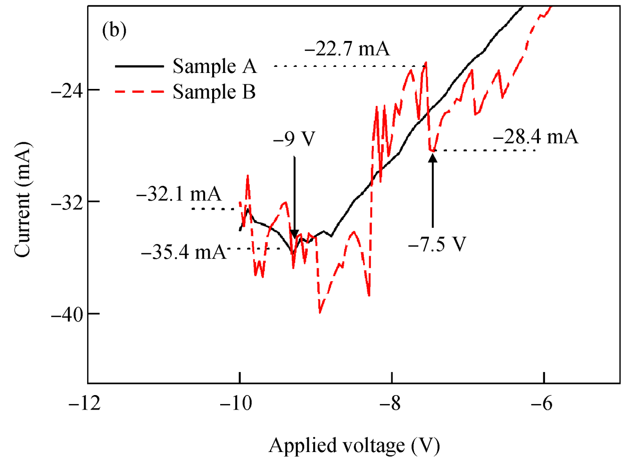

Fig. 3. (a) Current–voltage curves and (b) resonant tunnelling data under negative bias for samples A and B.

$$V_p \approx \frac{2(E_n - E_{c\text{-inj}})}{q}, \quad (3)$$

where h and $\hbar$ are plank and reduced plank constants; q and m^* are charge and effective mass of electron (we take $m^* \approx 0.6m_0$, m_0 is static mass of electron); k_x is the momentum parallel to the tunnelling direction and is quantized in the quantum well, which results in the energy level E_n quantized as in Eq. (2); $E_{c\text{-inj}}$ is the energy level of electrons injected from the electrode; n is the quantum number; and W_{well} is the width of the quantum well, equal to the nc-Si grain diameters according to the confinement crystallization principle, and these are 5 and 6 nm, respectively, for samples A and B.

In our experiments, the nc-Si grains function as a quantum well and are confined between SiO_2 sublayers, which function as tunneling barriers. Figure 4 is the energy band sketch of the structure. For samples A and B, the fabrication conditions are all the same, except for the oxidation time. This is 20 s for sample A and 10 s for sample B. This means that the thickness of the SiO_2 sublayers is greater for sample A than B ($W_A > W_B$), and the thickness of the nc-Si grains sublayers is smaller for A than B ($W_{wellA} = 5$ nm $< W_{wellB} = 6$ nm). So the first quantized energy level E_{1A} ($n = 1$) in sample A is larger than that in sample B, E_{1B}, according to Eq. (2) (i.e. E_{1A} (0.05 eV) $>$ E_{1B} (0.035 eV)). $E_{c\text{-inj}}$ is equal to the sum of the work function

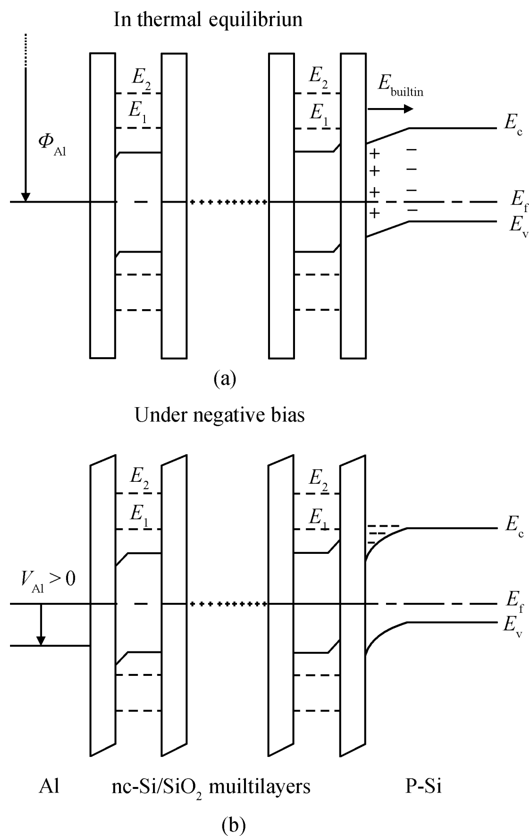

Fig. 4. Energy band diagram of the nc-Si/SiO_2 multilayers (a) in thermal equilibrium and (b) under negative bias.

Φ_{Al} for Al electrodes and the applied bias, and it is the same for samples A and B. So, from Eq. (3), V_p value for Sample A ($V_{pA} = 0.1$ V) is larger than V_{pB} ($V_{pB} = 0.07$ V). On the other hand, the SiO_2 sublayers are thicker for sample A, when applying bias, more voltage drops across the SiO_2 sublayers, so higher voltage is needed for sample A to increase the energy level from $E_{c\text{-inj}}$ to E_{1A}. Furthermore, the thicker SiO_2 results in a larger band width of the resonant tunneling band for sample B. Thus, V_p expressed in Eq. (3) is only the voltage drop across the electrode to the nearest nc-Si well, which is smaller than the measured values shown in Fig. 3. And the measured RTPV is the total voltage drop across the sample, and is related to the thicknesses of both the nc-Si and the SiO_2 sublayers.

Resonant tunnelling takes place also when negative bias is applied, but the RTPV is higher than that under forward bias for both samples A and B. This can be explained by the energy band diagram and the equivalent circuit diagram shown in Figs. 4 and 5. Here, it is supposed that an ohmic contact was formed between the Al electrode and the p-Si substrate. The work function of the Al electrode, nc-Si and p-Si substrate are about 4.25, 4.60 and 4.99 eV, respectively. When there is no applied voltage across the structure, their Fermi levels line up in thermal equilibrium by band bending, as shown in Fig. 4(a). Holes accumulate at the interface of the p-Si substrate and the first SiO_2 sublayer, leaving a negative stationary charge in the body. This forms the built-in electric field directed from the interface to the body, as shown in Fig. 4(a). The energy band structure resembles that of the PN junction, except that no carriers diffuse over the SiO_2 barriers. In the equivalent circuit diagram in Fig. 5, a diode with a tilde mark called the semblable diode is used to stand for the function of the above band bending. The nc-Si/SiO_2 multilayers of eight periods are treated as a variable resistance, whose resistivity drops greatly when resonant tunnelling occurs.

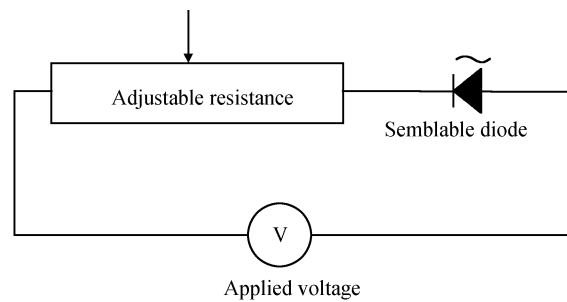

Fig. 5. Equivalent circuit diagram of the sample under bias.

When forward bias is applied, the diode turns on, and as the energy level of the electrons in the Al electrode is the same as that of the first quantized energy level in the nearest quantum well, resonant tunneling takes place.

When negative bias is applied, the holes accumulated at the interface are firstly drawn back to the body and then, with increasing the bias, depletion occurs at the interface. If the bias is increased further, inversion will occur, as shown in Fig. 4(b). The minority (i.e. electrons) will be collected at the interface. When the bias is high enough to power the electrons with energy equal to the quantized energy level in the nearest quantum well, resonant tunneling happens. So, the RTPV under negative bias is higher than that under forward bias for both samples.

4. Conclusions

In conclusion, carrier transportation in nc-Si/SiO_2 mulitlayers fabricated in a PECVD system was characterized by current voltage measurement. Resonant tunnelling was observed under both forward and negative biases at room temperature. The RTPV is related to the thicknesses of SiO_2 and nc-Si sublayers. The thicker the SiO_2 and the thinner the nc-Si, the higher the RTPV. On the other hand, the RTPV under negative bias is larger than that under forward bias. An energy band sketch and equivalent circuit diagram were constructed to analyze the transport processes. Under negative bias, the energy band of the p-Si substrate was firstly flattened, then depleted, and even inversed at the interface with increasing bias. If the bias is high enough to power the electrons collected at the interface to gain energy equal to the quantum energy level in the well, resonant tunnelling through the SiO_2 barrier occurs.

Acknowledgement

I wish to express my appreciation to Liu Yu from Nanjing University for her help in sample fabrication.

References

[1] Pavesi L. Silicon-based light sources for silicon integrated circuits. Adv Opt Technol, 2008, 2008: 416926
[2] Soref R. The past, present, and future of silicon photonics. IEEE J Sel Topics Quantum Electron, 2006, 12(6): 1678

[3] Daldosso N, Pavesi L. Nanosilicon photonics. Laser & Photonic Review, 2009, 3(6): 508

[4] Heitmann J, Muller F, Zacharias M, et al. Silicon nanocrystals: size matters. Adv Mater, 2005, 17(7): 795

[5] Hirose M, Mizubayashi W, Khairurrijal, et al. Ultrathin gate dielectrics for silicon nanodevices. Superlattices and Microstructures, 2000, 27(5): 383

[6] Horvath Z J. Semiconductor nanocrystals in dielectrics: optoelectronic and memory applications of related silicon-based MIS devices. Current Applied Physics, 2006, 6(2): 145

[7] Park N M, Kim S H, Maeng S, et al. High negative differential resistance in silicon quantum dot metal–insulator–semiconductor structure. Appl Phys Lett, 2006, 89(15): 153117

[8] Pei Z, Su A Y K, Hwang H L, et al. Room temperature tunnelling transport through Si nanodots in silicon rich silicon nitride. Appl Phys Lett, 2005, 86(6): 063503

[9] Wu L C, Chen K J, Wang J M, et al. Charge retention enhancement in stack nanocrystalline-Si based metal–insulator–semiconductor memory structure. Appl Phys Lett, 2006, 89(11): 12118

[10] Slight T J, Romeira B, Wang L A, et al. Lienard oscillator resonant tunneling diode-laser diode hybrid integrated circuit: model and experiment. IEEE J Quantum Electron, 2008, 44(12): 1158

[11] Jin N, Chung S Y, Yu R, et al. The effect of spacer thicknesses on Si-based resonant interband tunneling diode performance and their application to low-power tunneling diode SRAM circuits. IEEE Trans Electron Devices, 2006, 53(9): 2243

[12] Chen D Y, Wei D Y, Xu J, et al. Enhancement of electroluminescence in p–i–n structures with nano-crystalline Si/SiO_2 multilayers. Semicond Sci Technol, 2008, 23(1): 015013

[13] Campbell I H, Fauchet P M. The effects of microcrystal size and shape on the one phonon Raman spectra of crystalline semiconductors. Solid State Commun, 1986, 58: 739

[14] Sopinskyy M, Khomchenko V. Electroluminescence in SiO_x films and SiO_x-film-based systems. Current Opinion in Solid State and Materials Science, 2003, 7(2): 97

[15] Sze S M, Kwok N K. Physics of semiconductor devices. Hoboken, New Jersey: John Wiley & Sons, 2007: 346